Supporting Information for

Physical basis for long-distance communication along meiotic chromosomes

Kyle R. Fowler, Randy W. Hyppa, Gareth A. Cromie, and Gerald R. Smith

Supplemental materials and methods

Analysis of DNA proximity by chromosome-conformation capture

DNA isolation. Cells from 500 ml of culture were harvested 3.5 hr after meiotic induction, washed in cold PBS, and incubated in 1% formaldehyde (Sigma) for 5 min at 25°C. Cross-linked cells were opened using a Bead-beater (BioSpec), the chromatin solubilized using a water-bath sonicator (BioRuptor) and centrifuged at 4°C, and the supernatants removed for immunopreciptiation (1). Each chromatin sample was split into two immunoprecipitations, which used magnetic Protein-G beads (Invitrogen) pre-bound with appropriate antibody and incubated with chromatin for 2 hr with rotation at 25°C. Each IP was washed 3x with PBS before being resuspended in 1x Klenow buffer (NEB) supplemented with dNTPs, ATP, and 5 U of Klenow fragment of DNA polymerase I (3' → 5' exo$^-$; NEB) to create blunt ends on the DNA. One of the two IPs was ligated by resuspending the beads in 1 mL of 1x NEB Buffer 2 supplemented with 1 mM ATP and 400 U of T4 ligase (NEB) and incubating with rotation overnight at 4°C; the supernatant was removed and replaced with buffer and 400 U of T4 ligase as before, and incubation continued 2 hr more. Chromatin was eluted twice by incubating the beads in 100 µL of 1% SDS for 15 min at 65°C with frequent vortexing. The second (un-ligated) IP was eluted as above immediately after the binding, washing, and Klenow incubation steps without ligation. For both IPs, formaldehyde cross-links were removed by incubating eluates overnight at 75°C. Protein was subsequently removed using 2 µL of Proteinase K (Invitrogen; 20 mg/mL), and the DNA purified by phenol-chloroform extraction and treatment with RNase A overnight. DNA was cleaned using a PCR purification kit (Qiagen). To the DNA from the second (un-ligated) IP, buffer and 400 U of T4 ligase were added as above and incubated with rotation overnight at 4°C; additional ligase was added as above and incubated 2 hr further before being cleaned using a PCR purification kit (Qiagen). DNA from all samples was amplified using either a Sequenase Version 2.0 DNA Sequencing Kit (for anti-GFP) or a Qiagen REPLI-g Single Cell Kit (for anti-FLAG). DNA was quantified using a Bioanalyzer (Invitrogen).

High-throughput sequencing. Sequencing libraries were each prepared from 1 µg of DNA. DNA was initially fragmented with a Covaris LE220 Focused-ultrasonicator (Covaris, Woburn,

www.pnas.org/cgi/doi/10.1073/pnas.1801920115

MA) using factory settings for an average size of 300 bp. Library DNA was prepared using the KAPA DNA Library Preparation and HiFi PCR Kits (Kapa Biosystems, Wilmington, MA) on a PerkinElmer Sciclone NGSx Workstation (PerkinElmer, Waltham, MA) for Rec25-FLAG and Rec27-FLAG IPs, or the Epicentre Nextera DNA Sample Prep kit (Illumina, Inc., San Diego, CA) manually for Rec27-GFP IPs.

Library DNA size distributions were validated using an Agilent 2200 TapeStation (Agilent Technologies, Santa Clara, CA) and quantified with a Caliper/PerkinElmer LabChip DS spectrophotometer. Additional quality control, blending of pooled indexed libraries, and cluster optimization were performed using Life Technologies' Invitrogen Qubit® 2.0 Fluorometer (Life Technologies-Invitrogen, Carlsbad, CA). Individual indexed libraries were either pooled (4-plex, Rec27-GFP IPs) and clustered onto a single High Output Run flow cell, or pooled (6-plex, Rec25-FLAG and Rec27-FLAG IPs) and clustered onto two lanes of an Illumina Rapid Run v1 flow cell using an Illumina cBot. Sequencing was performed using either an Illumina HiSeq 2000 in High Output Run mode or Illumina HiSeq 2500 in Rapid Run mode using v1 reagents, employing a paired-end, 50-base read length (PE50) sequencing strategy.

Image analysis and base-calling were performed using Illumina's Real Time Analysis software (either v1.12.4 or v1.17.21.3), followed by "demultiplexing" of indexed reads and generation of FASTQ files, using Illumina's CASAVA software (either v1.8.0 or 1.8.2) (http://support.illumina.com/sequencing/sequencing_software/casava.html).

Sequence read mapping. Sequences from each paired-end read were independently mapped to the *S. pombe* genome (downloaded August 2010) using the Burrows-Wheeler Aligner (BWA, v 0.7.9a; (2)) and output as SAM files. We conservatively allowed only a single mismatch per 49 bp sequence (bp 50 was trimmed due to its high inherent error) and kept only sequence pairs where both ends mapped to a single chromosomal position (*i.e.,* a single possible locus of origin). Furthermore, both sequences of a pair had to map to the same chromosome. Alignment files were subsequently imported into R (http://www.r-project.org/) using the Rsamtools package (3) and analyzed using the BioStrings (4) and GenomicRanges (5) packages. Because ~1/3 of each DNA molecule was sequenced (50 bp read per end of each ~300 bp fragment), a significant fraction of all ligation junctions was sequenced. Such molecules would produce a chimeric sequence read, with the 5` portion reflecting one genomic locus and the 3` end another, and would fail to map to the genome based upon our stringent criteria. To capture such events, we iteratively mapped reads failing to map to the genome by trimming the sequence and re-mapping: initially all 49 bp were used, then the 5`-most 25 bp, then the 3`-most 34 bp, and finally the 5`-most 15 bp. Reads that successfully mapped to a single position in the genome were kept, while those that failed were passed to the next iteration;

those that failed to map (or mapped to multiple places) after trimming to 15 bp were set aside. Read-pairs that successfully mapped to the genome after these iterations were pooled and used in subsequent analyses and plots. The results reported here were validated using only reads that mapped on the first iteration (*i.e.,* using all 49 bp).

Filtering intra-molecular interactions. DNA ligation events are relatively rare, with most sequences being of non-ligated DNA. These read-pairs reflect the length of the DNA molecules in the sequencing libraries (~300 bp), while all inter-molecular ligations will give rise to molecules with a larger apparent size. Most ligation events are predicted to arise from intra-molecular interactions (*i.e*., DNA circularization, based upon the close proximity of sonicated DNA ends), and should be removed from further analysis. The map distance between sequence read-pairs derived from circularized molecules reflects the length of sheared meiotic chromatin, the DNA length at the time of ligation. Thus, filtering reads with an apparent length less than the shear length of meiotic chromatin will remove reads of non-ligated and intra-molecular ligation products. To this end, we determined the length distribution of the DNA molecules at the time of ligation by analyzing the map distance between paired reads that map to the same DNA strand (Figure S6A). Such molecules must have arisen from the ligation of DNA ends, of separate molecules, many of which are very distant in the linear genome (Figure S6B). We next binned all paired reads based on their map distance (*e.g.,* reads <200 bp apart, <300 bp, *etc*.) and plotted the fraction of each bin that mapped to the same strand and therefore arose by ligation (Figure S6C). Very close sequence pairs (<300 bp) almost exclusively map to opposite strands, as expected for sequencing primarily intact DNA duplexes (*i.e.,* unligated DNA). Longer reads, up to ~2 kb, are a mixture of same and opposite-stranded reads due to both inter- and intra-molecular ligations, respectively. ~50% of pairs very far apart (>2 kb) are same-stranded due to their arising almost exclusively from inter-molecular ligations, which can give rise to either sequence orientation with equal probability (unlike intra-molecular ligations); the other ~50% also result from inter-molecular ligations but in the other orientation and thus give rise to opposite-strand sequences. Together, these results indicate that sequence pairs <2 kb are biased by intra-molecular interactions. Note that this suggests a DNA size distribution (with most DNA <2 kb), which agrees well with previous results using identically sheared DNA. In all subsequent analyses, paired reads with a map distance <2 kb were excluded.

Hotspot interactions. Positions of published DSB hotspots in *S. pombe* (6) were used to identify sequence pairs where one, both, or neither paired-end read corresponded to hotspot DNA. Sequence-read map positions were compared with hotspot start and end positions, and sequences where at least one end came from a hotspot were pooled. Sequence pairs mapping to different hotspots indicated hotspot interactions; pairs where only one sequence mapped to hotspot DNA, and

the other to cold DNA, may reflect strong competition (*e.g*., sites around *mbs1* or *ade6-3049* where breakage is apparent only in the absence of these hotspots and thus were considered cold DNA).

We first assessed these interactions by looking at an individual hotspot, *ade6-3049* (Figures 1B and 4B). We used the published hotspot start and end positions, ± 2 kb to account for the sheared DNA maximal length, and identified sequence pairs where at least one read mapped inside the hotspot. A cumulative curve was generated from these reads based upon the distance between paired ends (Figure 4D). This was repeated for all hotspots in the genome, and the mean cumulative distribution determined (Figure 4F). This aggregate hotspot analysis was repeated using each sequencing dataset (Figure 4F and Figure S6D).

We next performed a statistical analysis on different subsets of hotspot-associated sequence pairs based upon the distance between reads and whether or not the paired sequence is also from a hotspot. We first identified sequences within ± 2 kb of each hotspot in the genome and grouped these based upon where the other paired sequence mapped (in a hotspot or in a cold-region) and its distance (<100 kb or >100 kb). For each hotspot, the number of sequences in each group (*e.g.,* pairs with one read in the hotspot being analyzed and the other in a hotspot <200 kb away) was normalized by the frequency expected if the paired ends were randomly placed in the appropriate vicinity (*e.g*., the fraction of DNA that occurs in hotspots within a 200 kb interval around the hotspot being analyzed). This procedure accounts for cold-region DNA being much more abundant genome-wide and that 200 kb, a small fraction of each chromosome, should contribute relatively few interactions compared to the rest of the chromosome. The interaction frequencies of each group were then compared using a paired t-test to determine statistical significance (Figure 4G).

Construction of *mbs1-20* deletion

Oligonucleotides 1018 and 1019 were used with *S. pombe* genomic DNA as template to make a PCR product ~500 bp long at the left end of the *mbs1-20* deletion; a similar PCR product at the right end was generated using oligonucleotides 1021 and 1022 with *S. pombe* genomic DNA as template. Oligonucleotides 1019 and 1021 are complementary. The two PCR products, plus oligonucleotides 1018 and 1022, were used to generate a PCR product ~1 kb long, which was used to transform strain GP4126 (*mbs1-1::ura4*$^{+}$) to 5-fluoro-orotic acid (FOA)-resistance. A transformant, GP4253, was purified and confirmed by nucleotide sequence analysis to contain the 6.6 kb deletion designated *mbs1-20*, which was transferred from GP4253 to other strains by meiotic crosses.

Construction of *rec25::FLAG* and *rec27::FLAG* alleles

DNA oligos with 80 bp of homology to the left and right of the ORF of either *rec25* (OL3169 and OL3170) or *rec27* (OL3171 and OL3172) were used to amplify a *2FLAG-kanMX6* cassette sequence from *S. pombe* strain GP7932 (*cnp20-2FLAG::kanM6*). The resulting PCR products were purified and used to transform *S. pombe* strain GP5623 to G418-resistance on YEA (7). The alleles *rec25-221::2FLAG-kanMX6* in strain GP8112 and *rec27-222::2FLAG-kanMX6* in strain GP8113 were verified by PCR and sequencing; they were transferred to other strains by meiotic crosses.

References

1. Fowler KR, Gutiérrez-Velasco S, Martín-Castellanos C, & Smith GR (2013) Protein determinants of meiotic DNA break hotspots. *Mol. Cell* 49:983-996.
2. Li H & Durbin R (2009) Fast and accurate short read alignment with Burrows-Wheeler transform. *Bioinformatics* 25(14):1754-1760.
3. Morgan MT, Pagès H, Obenchain V, & Hayden N (2016) Rsamtools: Binary alignment (BAM), FASTA, variant call (BCF), and tabix file import. R package version 1.24.0.
4. Pagès H, Aboyoun P, Gentleman R, & DebRoy S (2016) Biostrings: String objects representing biological sequences, and matching algorithms. R package version 2.40.2.
5. Lawrence M*, et al.* (2013) Software for computing and annotating genomic ranges. *PLoS Comput Biol* 9(8):e1003118.
6. Fowler KR, Sasaki M, Milman N, Keeney S, & Smith GR (2014) Evolutionarily diverse determinants of meiotic DNA break and recombination landscapes across the genome. *Genome Research* 24:1650-1664.
7. Bähler J*, et al.* (1998) Heterologous modules for efficient and versatile PCR-based gene targeting in *Schizosaccharomyces pombe*. *Yeast* 14:943-951.
8. Smith GR (2009) Genetic analysis of meiotic recombination in *Schizosaccharomyces pombe*. *Meiosis,* Methods in Molecular Biology, ed Keeney S (Humana Press, Totowa, NJ), pp 65-76.
9. Zahn-Zabal M, Lehmann E, & Kohli J (1995) Hot spots of recombination in fission yeast: inactivation of the *M26* hot spot by deletion of the *ade6* promoter and the novel hotspot *ura4-aim*. *Genetics* 140:469-478.
10. Baur M*, et al.* (2005) The meiotic recombination hot spot *ura4A* in *Schizosaccharomyces pombe*. *Genetics* 169(2):551-561.
11. Steiner WW & Smith GR (2005) Optimizing the nucleotide sequence of a meiotic recombination hotspot in *Schizosaccharomyces pombe*. *Genetics* 169(4):1973-1983.
12. Tanaka K, Chang HL, Kagami A, & Watanabe Y (2009) CENP-C functions as a scaffold for effectors with essential kinetochore functions in mitosis and meiosis. *Developmental cell* 17(3):334-343.
13. Cromie GA, Rubio CA, Hyppa RW, & Smith GR (2005) A natural meiotic DNA break site in *Schizosaccharomyces pombe* is a hotspot of gene conversion, highly associated with crossing over. *Genetics* 169:595-605.
14. Iino Y & Yamamoto M (1985) Mutants of *Schizosaccharomyces pombe* which sporulate in the haploid state. *Molecular and General Genetics* 198:416-421.
15. Guerra-Moreno A, Alves-Rodrigues I, Hidalgo E, & Ayte J (2012) Chemical genetic induction of meiosis in *Schizosaccharomyces pombe*. *Cell Cycle* 11(8):1621-1625.
16. Farah JA, Hartsuiker E, Mizuno K-I, Ohta K, & Smith GR (2002) A 160-bp palindrome is a Rad50•Rad32-dependent mitotic recombination hotspot in *Schizosacchromyces. pombe*. *Genetics* 161:461-468.

17. Farah JA, Cromie G, Davis L, Steiner WW, & Smith GR (2005) Activation of an alternative, Rec12 (Spo11)-independent pathway of fission yeast meiotic recombination in the absence of a DNA flap endonuclease. *Genetics* 171(4):1499-1511.
18. Davis L & Smith GR (2003) Non-random homolog segregation at meiosis I in *Schizosaccharomyces pombe* mutants lacking recombination. *Genetics* 163:857-874.
19. Davis L, Rozalén AE, Moreno S, Smith GR, & Martin-Castellanos C (2008) Rec25 and Rec27, novel components of meiotic linear elements, link cohesin to DNA breakage and recombination in fission yeast. *Current Biology* 18:849-854.
20. Grimm C, Bahler J, & Kohli J (1994) *M26* recombinational hotspot and physical conversion tract analysis in the *ade6* gene of *Schizosaccharomyces pombe*. *Genetics* 135:41-51.
21. Hyppa RW & Smith GR (2009) Using *Schizosaccharomyces pombe* meiosis to analyze DNA recombination intermediates. *Meiosis,* Methods in Molecular Biology, ed Keeney S (Humana Press, Totowa, NJ), pp 235-252.
22. Hyppa RW, Cromie GA, & Smith GR (2008) Indistinguishable landscapes of meiotic DNA breaks in *rad50*$^{+}$ and *rad50S* strains of fission yeast revealed by a novel *rad50*$^{+}$ recombination intermediate. *PLoS Genet* 4(11):e1000267.
23. Cromie GA*, et al.* (2007) A discrete class of intergenic DNA dictates meiotic DNA break hotspots in fission yeast. *PLoS Genetics* 3:e141.

Table S1. Positive DSB interference in *tel1*$^{+}$ strains but negative DSB interference in *tel1Δ* strains: interference weakens with distance in the 15 – 250 kb range.

		***tel1*$^{+}$**					***tel1Δ***				
Distance between hotspots (kb)[1]	**Supple-mental Figure**	**DSB1**	**DSB2**	**2X cut obs**	**2X cut exp**	**I**	**DSB1**	**DSB2**	**2X cut obs**	**2X cut exp**	**I**
15-20	Figure 3 B&C[2]	5.8 +/-0.26	9.0 +/-0.55	0.2 +/-0.1	0.52 +/-0.05	0.64 +/-0.14	6.0 +/-0.38	11.8 +/-0.58	2.6 +/-0.39	0.71 +/-0.08	-2.6 +/-0.32
	3 B&C	5.8	8.0	0.1	0.46	0.81	9.4	10.0	2.1	0.90	-1.3
	3 D&E	6.1 +/-0.48	8.8 +/-0.86	0.1 +/-0.009	0.53 +/-0.09	0.84 +/-0.04	5.9 +/-0.40	10.5 +/-0.18	2.4 +/-0.31	0.62 +/-0.05	-3.0 +/-0.75
20-25 (*ura2-leu2*)	5 B (a – b)[3]	4.92 +/-0.56	5.05 +/-0.68	0.12 +/-0.002	0.25 +/-0.06	0.52 +/-0.05	5.0 +/-0.39	5.26 +/-0.65	0.58 +/-0.058	0.26 +/-0.04	-1.32 +/-0.43
45	3 B&C	ND[4]					7.3	7.7	2.5	0.56	-3.5
	3 D&E						3.8	6.6	1.1	0.25	-3.4
95	5 B (a – c)	4.92 +/-0.56	11.42 +/-0.93	0.83 +/-0.006	0.57 +/-0.1	-0.61 +/-0.45	5.0 +/-0.39	12.75 +/-0.55	1.92 +/-0.34	0.64 +/-0.007	-2.16 +/-0.87
100 (*mbs1-2*)	5 A (*mbs1-2*)	10.43 +/-1.03	3.3 +/-0.18	0.18 +/-0.02	0.35 +/-0.05	0.46 +/-0.06	13.16 +/-0.26	4.38 +/-0.22	0.49 +/-0.009	0.59 +/-0.04	0.16 +/-0.07
125	5 D (d – e)	3.6	9.3	0.31	0.33	0.06	3.2	11.9	0.8	0.38	-1.1
		3.3	8.8	0.20	0.29	0.31	3.1	11.7	0.55	0.36	-0.5
250	5 D (f – g)	7.1	8.7	0.40	0.62	0.35	8.0	11.7	0.89	0.94	0.05
		8.1	10.0	0.54	0.81	0.33	8.5	15.9	0.80	1.3	0.38

[1] Distances were determined from the genome-wide analysis of DSB hotspots (1, 6) and the *S. pombe* genome sequence (https://www.pombase.org/).

[2] Main text Figure 3B and 3C.

[3] DSB hotspot pairs assayed for double-cut fragments are in parentheses.

[4] The 45 kb interval could not be measured because the left DSB hotspot is created by *tel1Δ*.

Data are the percent of total DNA cut at each hotspot (DSB1 and DSB2) and at both hotspots (2X cut obs). 2X cut exp is the percent cut at both hotspots expected from independent breakage (DSB1 times DSB2). Interference I = 1 – (2x cut obs/2x cut exp). Data are from the experiments shown in

the indicated figures. Values are mean ± SEM for three or more determinations, or individual values for one or two determinations.

Table S2. Crossover interference

A. Intra-chromosomal interference – strongly negative in *tel1Δ* mutants and weakly positive in wild type

tel1	R_1	R_2	R_D	Expected R_D	CoC	I[a]
+	3.40	13.0	0.32	0.44	0.72	0.28
+	3.12	12.2	0.34	0.38	0.89	0.11
+	4.68	20.00	0.62	0.94	0.66	0.34
+	3.84	23.3	0.74	0.89	0.83	0.17
+	3.78	18.9	0.44	0.71	0.62	0.38
mean	3.76	17.5	0.49	0.67	0.74	**+0.26**
± SEM	± 0.26	± 2.1	± 0.08	± 0.11	± 0.051	**± 0.051**
Δ	3.26	8.84	0.56	0.29	1.93	-0.93
Δ	3.78	8.58	0.66	0.32	2.06	-1.06
Δ	3.16	10.0	0.56	0.32	1.75	-0.75
Δ	3.16	9.70	0.56	0.31	1.81	-0.81
Δ	2.66	6.54	0.30	0.17	1.76	-0.76
Δ	2.58	6.90	0.34	0.18	1.89	-0.89
Δ	2.78	5.86	0.34	0.16	2.13	-1.13
Δ	2.78	7.56	0.40	0.21	1.90	-0.90
mean	3.02	8.00	0.47	0.245	1.90	**-0.90**
± SEM	± 0.14	± 0.54	± 0.048	± 0.025	± 0.048	**± 0.048**

[a] In additional crosses conducted with different strains on different days (Table S2B and S2C and other crosses), I = 0.29 ± 0.043 (n = 12) for *tel1*$^+$ and -0.80 ± 0.14 (n = 8) for *tel1Δ.*

For part A. Crosses were conducted between strains GP77 and GP7144 (*tel1*$^+$) and between strains GP9019 and GP9022 (*tel1Δ*). Each pair had *ura2-10* + *lys7-2* and + *leu2-120* +, linked loci on chromosome I. Recombinant frequencies (twice the observed % of selected prototrophs among total viable spores) were determined by differential plating on appropriately supplemented NBA minimal medium. In the tested subset of both wt and *tel1Δ* crosses, ~10% of the double recombinants were complementing diploids (iodine-staining positive) (8). Thus, R_D and CoC may be ~5% less than shown here, and I would be about +0.27 for wt and about -0.92 for *tel1Δ*. This minor correction would not change our conclusions. More than 22 and usually more than 100 colonies were counted for each determination. The coefficient of coincidence (CoC) is $R_D/(R_1 \times R_2)$, where R_1 is twice the frequency of Ura$^+$ Leu$^+$ recombinants, R_2 is twice the frequency of Leu$^+$ Lys$^+$ recombinants, and R_D is twice the frequency of Ura$^+$ Leu$^+$ Lys$^+$ recombinants. Expected R_D is $(R_1 \times R_2)$. Interference (I) is 1 - CoC. These data are summarized in Table 1.

B. No significant inter-chromosomal crossover interference – *tel1*$^+$

Interval 3 (Chr 2)	CO interval 1 (%)	CO interval 2 (%)	CO interval 3 (%)	Double CO 1 and 2 (%)	Double CO 1 and 3 (%)	Double CO 2 and 3 (%)
ade7 – arg6	2.70 ± 0.060	11.52 ± 0.82	11.24 ± 0.90	0.232 ± 0.050	0.290 ± 0.035	1.25 ± 0.060
Interference				**0.24** ± 0.07	**0.04** ± 0.17	**0.03** ± 0.16
arg4 – arg5	2.62 ± 0.114	9.52 ± 0.48	4.64 ± 0.066	0.172 ± 0.012	0.127 ± 0.017	0.420 ± 0.052
Interference				**0.31** ± 0.04	**- 0.04** ± 0.13	**0.05** ± 0.11

C. No significant inter-chromosomal crossover interference – *tel1Δ*

Interval 3 (Chr 2)	CO interval 1 (%)	CO interval 2 (%)	CO interval 3 (%)	Double CO 1 and 2 (%)	Double CO 1 and 3 (%)	Double CO 2 and 3 (%)
ade7 – arg6	2.58 ± 0.16	7.36 ± 0.48	8.42 ± 0.096	0.344 ± 0.060	0.264 ± 0.017	0.668 ± 0.064
Interference				**-0.81** ± 0.25	**-0.22** ± 0.12	**-0.08** ± 0.11
arg4 – arg5	2.74 ± 0.26	6.50 ± 0.30	4.36 ± 0.13	0.316 ± 0.024	0.130 ± 0.014	0.278 ± 0.014
Interference				**-0.77** ± 0.17	**-0.09** ± 0.040	**0.02** ± 0.12

For parts B and C. Crosses were conducted between *tel1*$^+$ strains GP9443 and GP9445 (*ade7 – arg6*, linked loci on chromosome 2), between *tel1*$^+$ strains GP9453 and GP9449 (*arg4 – arg5,* linked loci on chromosome 2), between *tel1Δ* strains GP9442 and GP9444 (*ade7 – arg6*), and between *tel1Δ* strains GP9452 and GP9446 (*arg4 – arg5*); these strain pairs also contained the *ura2, leu2,* and *lys7* alleles linked on chromosome 1 as in part A. Recombinant frequencies were determined as in part A, except that differential plating was on appropriately supplemented PMG minimal medium. Recombinant frequencies for interval 1 and 3 (or 2 and 3) double recombinants are four times the

observed % of selected prototrophs among total viable spores. Except in a few cases, between 100 and 300 colonies were counted for each determination. Data are the mean ± SEM from four crosses with independent cultures.

Table S3. DSB frequencies at the *ura4A* and *ade6-3049* hotspots, alone and in combination.

DSB hotspot	+ + / - -	+ - / - +	+ - / + -	+ - / - -	- + / - +	- + / - -	+ + / + +
ura4A$^+$	1.8, 1.8, 1.45, 1.55 **1.65** ± 0.09	3.2, 3.05, 3.13, 2.87 **3.06** ± 0.07	6.3, 7.2, 6.25 **6.6** ± 0.3	4.0, 3.12, 3.65 **3.6** ± 0.3	0.2, 0.3, 0.1 **0.2** ± 0.06	0.2, 0.3, 0.1 **0.2** ± 0.06	1.4, 1.35, 2.1, 2.15 **1.75** ± 0.2
ade6-3049	8.9, 7.9, 9.0, 9.5 **8.83** ± 0.34	7.7, 7.8, 9.0, 9.1 **8.40** ± 0.38	0.1, 0.3, 0.1 **0.2** ± 0.07	0.3, 0.25, 0.1 **0.22** ± 0.06	12.2, 13.8, 14.9 **13.6** ± 0.8	5.55, 7.3, 5.6 **6.2** ± 1.0	13.2, 11.4, 18.2, 17.5 **15.1** ± 1.9
tel1::kanMX6	5.36, 4.38, 4.55, 4.80, 3.83, 2.87 **4.30** ± 0.35	5.0, 4.88, 5.80, 5.30, 3.70, 3.32 **4.67** ± 0.39		6.10, 4.05, 3.05 **4.40** ± 0.90		0.10, 0.40, 0.10 **0.20** ± 0.10	
ade6-3049	3.90, 3.01, 6.70, 4.50, 3.78, 4.22 **4.35** ± 0.51	7.51, 5.92, 10.60, 6.45, 5.65, 6.70 **7.14** ±0.74		0.15, 0.30, 0.1 **0.18** ± 0.06		7.28, 7.80, 5.30 **6.79** ± 0.76	

Strains induced for meiosis had the configuration of the *ura4A*, *tel1::kanMX6*, or *ade6-3049* hotspots shown in the top line as in Figure 2, *ura4A*$^+$ or *tel1::kanMX6* on the left and *ade6-3049* on the right. + indicates an active hotspot; - indicates no hotspot (lacking the *ura4A*$^+$ insertion or the *tel1::kanMX6* substitution, or containing the non-hotspot allele *ade6-3057*) (9, 10); (11). Data are the percent of total DNA broken at the *ura4A*$^+$*, tel1::kanMX6,* or *ade6-3049* hotspot determined in Southern blot hybridization analyses as in Figures 2 (top two sets of data) and S2 (bottom two sets of data). In bold is the mean, followed by the SEM.

Table S4. Genotypes of *S. pombe* strains.

Strain	Genotype[1]	Used in
GP7256	*h⁻/h⁻ ade6-3049/ade6-3049 pat1-114/pat1-114 rec27-205::GFP-kanMX6/rec27-205::GFP-kanMX6 rec12-169::kanMX6/rec12-169::kanMX6 his4-239/+ +/lys4-95*	Figures 1, 4, S8-S10
GP9246	*h+/h+ ade6-3049/ade6-3049 pat1-114/pat1-114 rec12-201::6His2FLAG/rec12-201::6His2FLAG rad50S/rad50S his4-239/lys4-95*	Figure 2
GP9305	*h+/h+ ade6-3049/ade6-3057 pat1-114/pat1-114 rec12-201::6His2FLAG/rec12-201::6His2FLAG rad50S/rad50S mbs1-20/+ his4-239/lys4-95*	Figures 2 and S2
GP9337	*h+/h+ ade6-3057/ade6-3049 +/ura4A pat1-114/pat1-114 rec12-201::6His2FLAG/+ rad50S/rad50S ura4-D18/ura4-D18 his4-239/lys4-95*	Figure 2
GP9338	*h+/h+ ade6-3057/ade6-3057 ura4A/ura4A pat1-114/pat1-114 rad50S/rad50S ura4-D18/ura4-D18 his4-239/lys4-95*	Figure 2
GP9339	*h+/h+ ade6-3049/ade6-3057 +/ura4A pat1-114/pat1-114 rec12-201::6His2FLAG/+ rad50S/rad50S ura4-D18/ura4-D18 his4-239/lys4-95*	Figure 2
GP9340	*h+/h+ ade6-3057/ade6-3057 +/ura4A pat1-114/pat1-114 rec12-201::6His2FLAG/+ rad50S/rad50S ura4-D18/ura4-D18 his4-239/lys4-95*	Figure 2
GP8828	*h^{90} rec10-203::GFP-kanMX6*	Figures 5 and S14
GP8824	*h^{90} rec25-204::GFP-kanMX6*	Figures 5 and S14
GP8826	*h^{90} rec27-205::GFP-kanMX6*	Figures 5 and S14
GP9036	*h^{90} rec10-203::GFP-kanMX6 tel1::kanMX6*	Figures 5 and S14
GP9033	*h^{90} rec25-204::GFP-kanMX6 tel1::kanMX6*	Figures 5 and S14
GP9034	*h^{90} rec27-205::GFP-kanMX6 tel1::kanMX6*	Figures 5 and S14
GP8907	*h⁺/h⁺ ade6-3049/ade6-3049 ura4⁺-aim/ura4⁺-aim pat1-114/pat1-114 tel1::kanMX6/tel1::kanMX6 rad50S/rad50S his4-239/+ +/lys4-95*	Figures 2, S2, S3 and S5
GP8908	*h⁻/h⁻ ade6-3049/ade6-3049 ura4⁺-aim/ura4⁺-aim pat1-114/pat1-114 rad50S/rad50S his4-239/+ +/lys4-95*	Figures S2, S3 and S5
GP8909	*h⁻/h⁻ ade6-3049/ade6-3049 ura4⁺-aim/ura4⁺-aim pat1-as1*(L95G)*/pat1-as1*(L95G) *rad50S/rad50S his4-239/+ +/lys4-95*	Figures 3, S2, S3, and S4
GP8910	*h⁻/h⁻ ade6-3049/ade6-3049 ura4⁺-aim/ura4⁺-aim pat1-as1*(L95G)*/pat1-as1*(L95G) *tel1::kanMX6/tel1::kanMX6 rad50S/rad50S his4-239/+ +/lys4-95*	Figures 3, S2, S3, and S4
GP8663	*h⁻/h⁻ ade6-3049/ade6-3049 pat1-114/pat1-114 rec27-205::GFP-kanMX6/rec27-205::GFP-kanMX6 rec8-176::kanMX/rec8-176::kanMX his4-239/+ +/lys4-95*	Figure 4 and S13
GP8237	*h⁻/h⁻ ade6-3049/ade6-3049 ura4-D18/+ pat1-114/pat1-114 rec12-171::ura4⁺/rec12-171::ura4⁺ rec25-221::2FLAG/rec25-221::2FLAG his4-239/+ +/lys4-95 +/leu1-32*	Figure S6
GP8240	*h⁻/h⁻ ade6-3049/ade6-3049 pat1-114/pat1-114 rec12-171::ura4⁺/rec12-171::ura4⁺ rec27-222::2FLAG/rec27-222::2FLAG his4-239/+ +/lys4-95 +/leu1-32*	Figure S6
GP7062	*h⁺/h⁺ ade6-3057/ade6-3057 pat1-114/pat1-114 rec12-201::6His-2FLAG/rec12-201::6His-2FLAG rad50S/rad50S lys4-95/+ +/his4-239*	Figures 1B, 1C, 1D, and S1
GP6852	*h⁺/h⁺ ade6-3049/ade6-3049 pat1-114/pat1-114 rec12-201::6His-2FLAG/rec12-201::6His-2FLAG rad50S/rad50S mbs1-20/mbs1-20 his4-239/+ +/lys4-95*	Figures 1B,1C, 1D, and S1
GP77	*h⁻ leu2-120*	Tables 1 and S2
GP7144	*h⁺ ura2-10 lys7-2*	Tables 1 and S2
GP9019	*h⁺ ura2-10 lys7-2 tel1::kanMX6*	Tables 1 and S2
GP9022	*h⁻ leu2-120 tel1::kanMX6*	Tables 1 and S2
GP9443	*h- ura2-10 lys7-2 arg6-328*	Table S2

GP9445	*h+ leu2-120 ade7-50*	Table S2
GP9453	*h+ ura2-10 lys7-2 arg5-189*	Table S2
GP9449	*h- leu2-120 arg4-55*	Table S2
GP9442	*h- ura2-10 lys7-2 arg6-328 tel1::kanMX6*	Table S2
GP9444	*h+ leu2-120 ade7-50 tel1::kanMX6*	Table S2
GP9452	*h+ ura2-10 lys7-2 arg5-189 tel1::kanMX6*	Table S2
GP9446	*h- leu2-120 arg4-55 tel1::kanMX6*	Table S2
GP4126	*h^+ ade6-3049 ura4-D18 mbs1-1::ura4$^+$ pat1-114 rad50S end1-458*	*mbs1-20* construction
GP9343	*h^+/h^+ ade6-3057/ade6-3049 pat1-114/pat1-114 rad50S/rad50S rec12-201::6His-2FLAG/rec12-201::6His-2FLAG +/tel1::kanMX6 his4-239/lys4-95 +/mbs1-20*	Figure S2
GP9344	*h^+/h^+ ade6-3057/ade6-3057 pat1-114/pat1-114 rad50S/rad50S rec12-201::6His-2FLAG/rec12-201::6His-2FLAG +/tel1::kanMX6 his4-239/lys4-95 mbs1$^+$/mbs1$^+$*	Figure S2
GP9345	*h^+/h^+ ade6-3049/ade6-3057 pat1-114/pat1-114 rad50S/rad50S rec12-201::6His-2FLAG/rec12-201::6His-2FLAG +/tel1::kanMX6 his4-239/lys4-95 mbs1-20/+*	Figure S2
GP7932	*h^- leu1 ade6 cnp20::2FLAG-kanMX6*	*rec25-221 and rec27-222* constructions
GP5623	*h^+ ade6-3049 ura4-D18 rec12-171::ura4$^+$*	*rec25-221 and rec27-222* constructions

[1] Strains were constructed by standard matings (8) or as described in Methods. Genealogies are available upon request. Sources of alleles, other than commonly used auxotrophies and *mat*, are the following: *ade6-3049* (11); *cnp20::2FLAG-kanMX6* (12); *mbs1-1::ura4*$^+$ (13); *mbs1-20* (Methods); *pat1-114* (14); *pat1-as1*(L95G) (15); *rad50S* (16); *rec8-176::kanMX* (17); *rec10-203::GFP-kanMX6* (1); *rec12-169::kanMX6* (18); *rec12-171::ura4*$^+$ (18); *rec25-204::GFP-kanMX6* (19); *rec25-221::2FLAG-kanMX6* (Methods); *rec27-205::GFP-kanMX6* (19); *rec27-222::2FLAG-kanMX6* (Methods); *tel1::kanMX6* (Y. Yamada, O. Limbo, P. Russell); *ura4A* (also called *ura4*$^+$*-aim* (20).

Table S5. Oligonucleotides.

Oligo number	Sequence (5' → 3')	Use
1401	GGATGGCTGCCCCTTCGTCTCG	Probe for Figure 2
1402	GGCTAACACTTATCAACGCG	Probe for Figure 2
2576	TTCCATCTTCAGCTCCCACT	Probe for Figures 3B and S2
2577	CGAGGACTTGCAATTGTCTG	Probe for Figures 3B and S2
2779	TGGTTTCTCTCAATCCCTTA	Probe for Figure S3
2780	TTACACACTTTACCCCGTTC	Probe for Figure S3
1018	GGCATAGTCCAATTCGCGCG	*mbs1-20* deletion
1019	GCTCACTTGCCCTAAGCTCACGTTCCCATAGGCCAGCAATTCCC	*mbs1-20* deletion
1021	GGGAATTGCTGGCCTATGGGAACGTGAGCTTAGGGCAAGTGAGC	*mbs1-20* deletion
1022	GCAATGGGCTTCGTGGGAGC	*mbs1-20* deletion
3126	AAGTATTAGAAGAAGATGGATCGCAGCAAGGGTCTCAGCTTATACA AGGGCTGCTAACGTGTTTTCAATCTACTGGTAATCGGATCCCCGGG TTAATTAA	Construction of *rec25-221::2FLAG-kanMX6*
3127	GACAATTAATAACATTTAGATGAAAAAGTAGTAGAGTTGGAATAAAT TTAGCTTTGAGTTTCAATCGTAATTTAGCTTATGAATTCGAGCTCGTT TAAAC	Construction of *rec25-221::2FLAG-kanMX6*
3128	GCAATCAGTTGTTACAGTATGCCGAGAAACTGCGAATTGTTGTTAAA ACCCCAATGAACCAACCAACAAATACAGAAGTACGGATCCCCGGGT TAATTA	Construction of *rec27-222::2FLAG-kanMX6*
3129	TAAATTGTATGCTCATAACATATTTTTAATTCGTTTTATGATTTTATGG CACTAGTTTATATAATGTGTTTAAAATGACTGAATTCGAGCTCGTTTA AAC	Construction of *rec27-222::2FLAG-kanMX6*

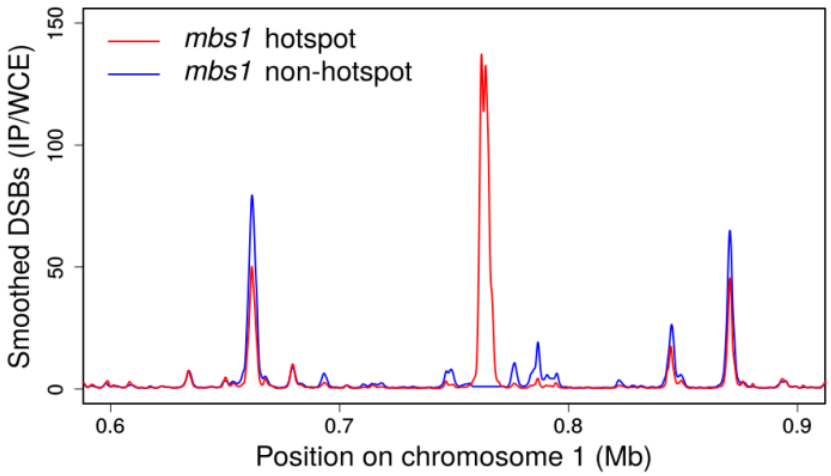

Figure S1. DSB competition and clustering at the natural DSB hotspot *mbs1* occur in *tel1*$^{+}$ cells. DSB frequency is reduced at hotspots within ~100 kb of the *mbs1* natural hotspot (13). See Figures 1 and 4 for further explanation. DSB frequency on part of chromosome 1 in *mbs1*$^{+}$ (wild-type) cells with a DSB hotspot (red line) and in the 6.6 kb *mbs1-20* deletion mutant without a hotspot (blue line). Data were median normalized separately (see Figure 1C). Note that low-level sites for DSBs in wild-type become stronger DSB hotspots in the absence of *mbs1*, a reflection of DSB competition.

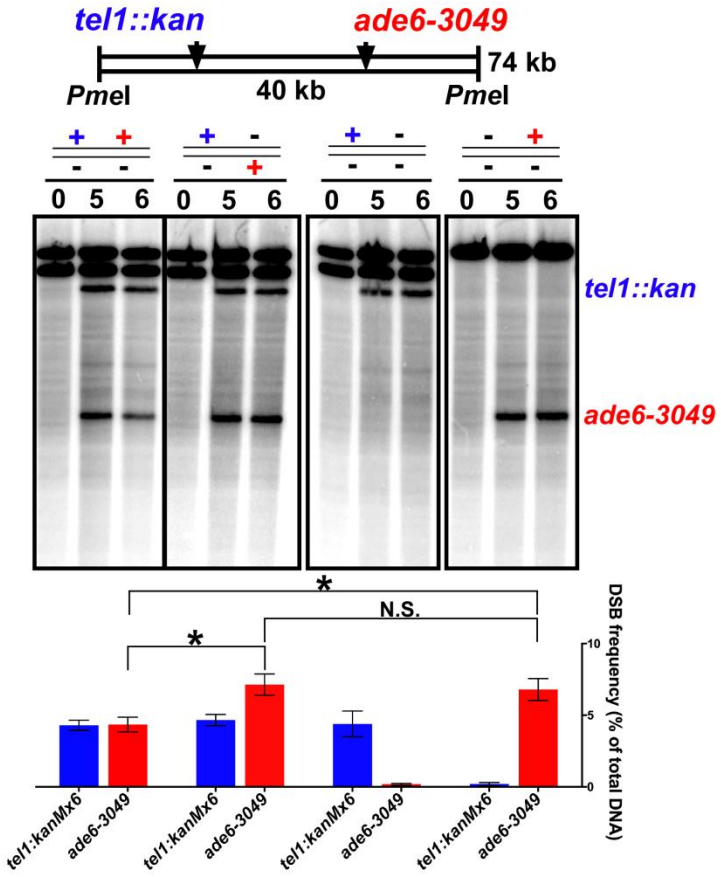

Figure S2. DSB competition acts along a homolog (in *cis*) but not between homologs (in *trans*). The *tel1::kan* (blue) and *ade6-3049* (red) DSB hotspots (+) were located either on the same parental homolog (in *cis*; left-most set of lanes) or on different parental homologs (in *trans*, second set of lanes); - indicates lack of a hotspot. In comparison experiments, one hotspot or the other was present in heterozygous condition (two right-most sets of lanes). Strains GP9343 (*tel1*::*kan ade6-3049/tel1*$^+$ *ade6*$^+$), GP9345 (*tel1*::*kan ade6*$^+$*/tel1*$^+$ *ade6-3049*), GP9344 (*tel1*::*kan ade6*$^+$*/tel1*$^+$ *ade6*$^+$) and GP9305 (*tel1*$^+$ *ade6-3049/tel1*$^+$ *ade6*$^+$) were induced for meiosis by raising the temperature to 34°C. DSBs at each hotspot were assayed at the indicated times after induction. Data (mean ± SEM; n = 3 to 6) are the percent of total DNA broken at the indicated hotspot (assayed with a probe at the right end of the *Pme*I fragment). Comparison of the fourth set of lanes (no *tel1::kan* hotspot) shows that the *ade6-3049* hotspot is significantly reduced when *tel1::kan* is in *cis* (first set of lanes; $p < 0.030$ by unpaired t-test; *) but not significantly reduced when *tel1::kan* is in *trans* (second set of lanes; $p = 0.78$ by unpaired t-test; N.S.). Direct comparison of the first two sets of lanes shows that *tel1::kan* reduces the *ade6-3049* hotspot significantly more in *cis* than in *trans* ($p < 0.011$ by unpaired t-test). See Table S3 for individual data.

\

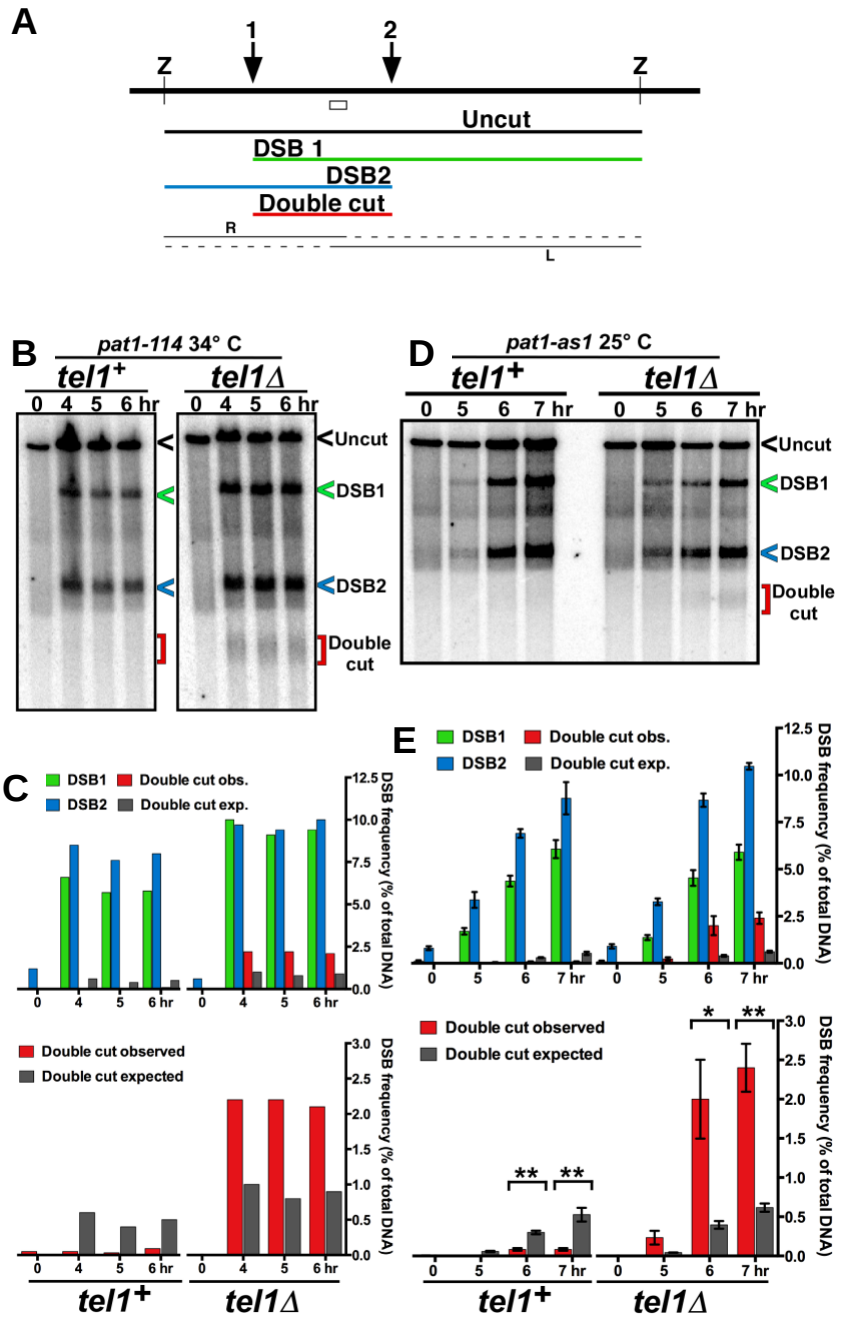

Figure S3. Interference of DSB formation at nearby hotspots depends on Tel1 DNA damage-response protein kinase: Analysis of two hotspots 15 kb apart near the left end of chromosome 2. (**A**) Scheme for determining DSB frequency at one, the other, and both hotspots (1 and 2) by Southern blot hybridization of DNA cut by a restriction enzyme Z; open box, probe position. The *rad50S* mutation, present in all strains, blocks DSB repair and allows their accumulation and quantification (21); DSBs accumulate in *rad50S* mutants with a distribution indistinguishable from that

of wild type (22). DNA fragments cut by Z at one end and by Rec12 at the other end (fragments DSB1 and DSB2) or at both ends by Rec12 (Double-cut fragment) migrate as distinct bands at the positions indicated (green and blue arrowheads for single-cut and red bracket for double-cut). DNA fragments cut at Z and mechanically broken during preparation in the region marked with a dotted line (bottom of scheme) migrate as a smear ending at the position corresponding to the DNA length from the probe to Z on the left or on the right (bands R and L, respectively). This feature accounts for the "rain" ending at distinct positions in the gel. Z was chosen so that the doubly-cut fragment migrates below the rain, enabling its quantification. (**B**) DSB interference between two hotspots on the left end of chromosome 2. Strains GP8908 (*pat1-114 tel1*$^{+}$) and GP8907 (*pat1-114 tel1Δ*) were induced by raising the temperature to 34°C. DNA was extracted at the indicated times, digested with *Avr*II (which cuts at bp 939346 and 993665), and analyzed by Southern blot hybridization using a 0.48 kb radioactive probe near the middle of the 54.3 kb fragment (uncut). (**C**) Quantification of the bands shows that the observed doubly-cut fragment (red bars) is less frequent than expected from independent breakage at the two hotspots (black bars) in wild type but more frequent than expected in *tel1Δ*. *, $p < 0.05$ by unpaired t-test; **, $p < 0.01$ by unpaired t-test. (**D**) Analysis as in panel B but with strains GP8909 (*pat1-as1 tel1*$^{+}$) and GP8910 (*pat1-as1 tel1Δ*) induced at 25°C with the adenine analog 3-MB-PP1 (15). (**E**) Analysis as in panel C of expected and observed double-cut fragments shown in panel D.

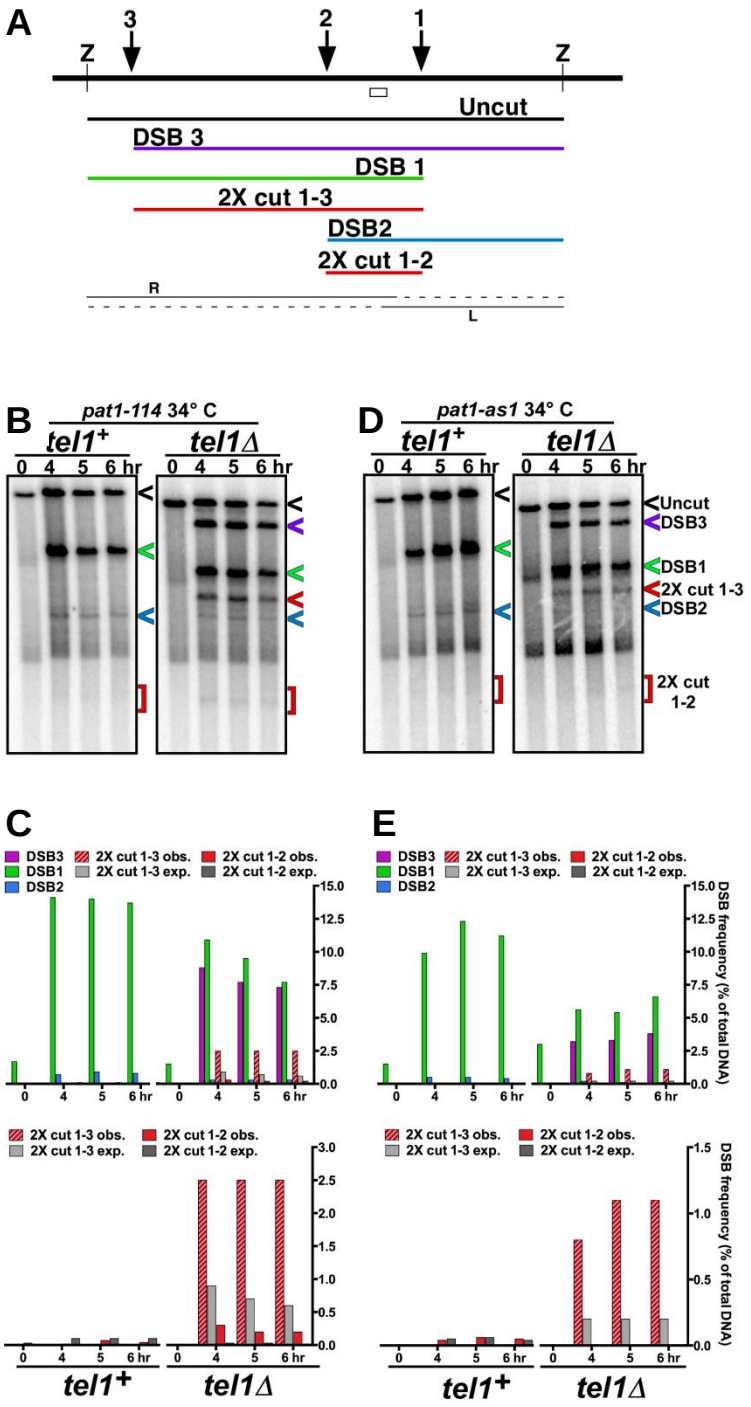

Figure S4. Interference of DSB formation at nearby hotspots depends on Tel1 DNA damage-response protein kinase: Analysis of two hotspots (in *tel1*$^{+}$) or three hotspots (in *tel1Δ*) near the middle of chromosome 3. DSB1 (in *ade6*) is ~16 kb from DSB2 (in *ura4A*) and ~45 kb from DSB3 (in *tel1::kanMX6*). (**A**) Scheme for determining DSB frequency at three hotspots (1, 2, and 3) near the middle of chromosome 3 by Southern blot hybridization of DNA cut by a restriction enzyme Z. See

Figure S3 for further explanation. (**B**) Strains GP8908 (*pat1-114 tel1*$^{+}$) and GP8907 (*pat1-114 tel1Δ*) were induced by raising the temperature to 34°C. DNA was extracted at the indicated times, digested with *Pme*I (which cuts at bp 1263677 and 1337886 in wt), and analyzed by Southern blot hybridization using a 0.75 kb radioactive probe near the middle of the 74.2 kb fragment (uncut; 66.3 kb in *tel1Δ*). (**C**) Quantification of the bands shows that the observed doubly-cut fragment (red bars) is less frequent than expected from independent breakage at the two hotspots (black bars) in wild type but more frequent than expected in *tel1Δ*. Note that the *tel1::kanMX6* mutation, about 45 kb to the left of the *ade6-3049* DSB hotspot, in strains GP8907 and GP8910 introduces a strong DSB hotspot, characteristic of such *kanMX6* insertions (23), giving rise to DSB3. (**D**) Analysis as in panel B but with strains GP8909 (*pat1-as1 tel1*$^{+}$) and GP8910 (*pat1-as1 tel1Δ*) induced at 34°C with the adenine analog 3-MB-PP1 (15). (**E**) Analysis as in panel C of expected and observed double-cut fragments shown in panel D.

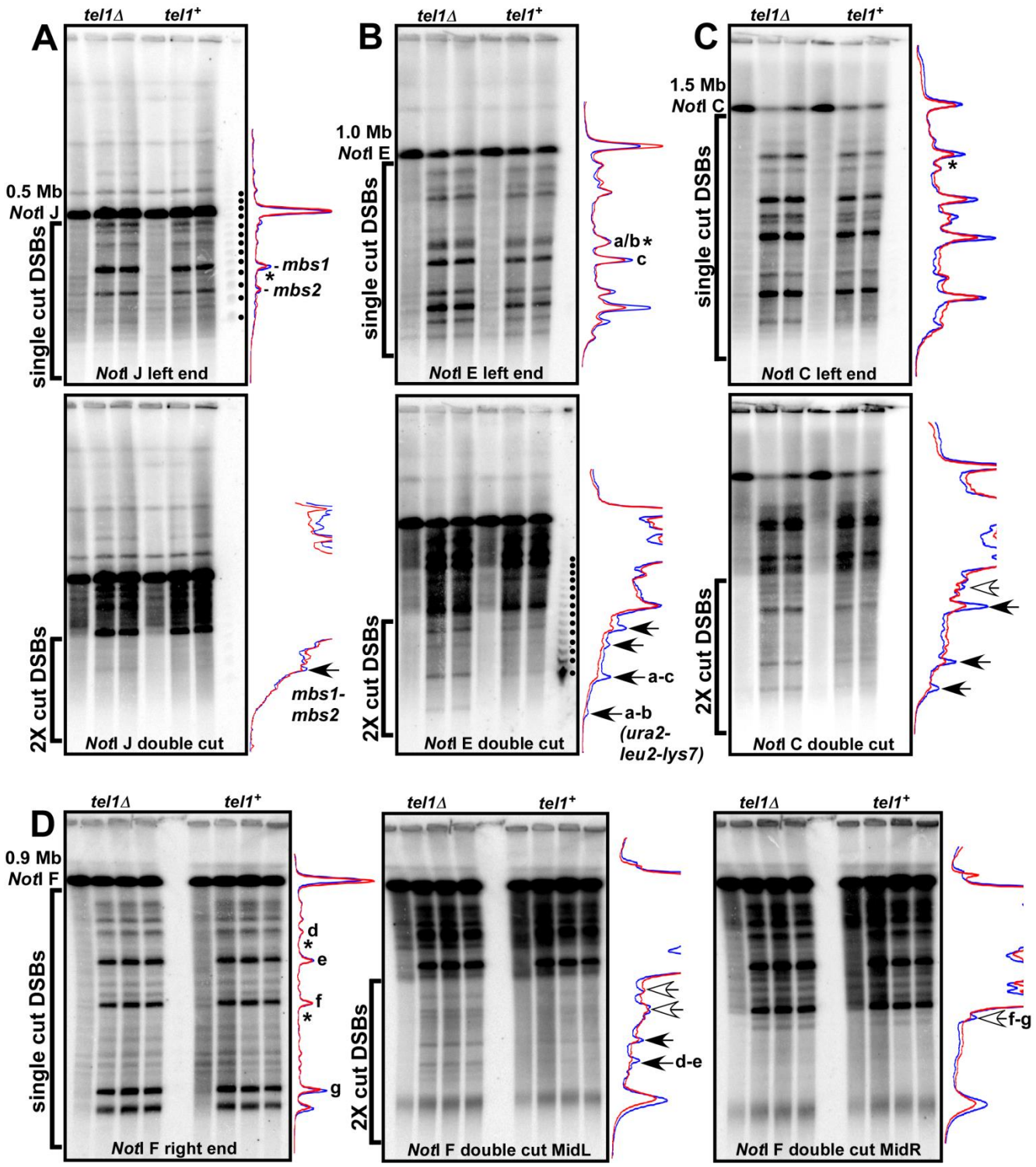

Figure S5. Interference of DSB formation at nearby hotspots depends on Tel1 DNA damage-response protein kinase: Analysis of DSBs at hotspots on *Not*I fragments on chromosomes 1 and 2. Shown are Southern blots with a probe from an end (for single cuts) or from the middle (for double cuts) of each fragment in *tel1Δ* (left three lanes) or in *tel1*$^{+}$ (right three lanes). Each set of three lanes

analyzes DNA from *pat1-114* cells harvested at 0, 5, and 6 hr after meiotic induction at 34°C; panel D has an additional time point at 4 hr. Lane traces to the right of each Southern blot are for *tel1Δ* (blue trace) or *tel1*$^{+}$ (red trace). Phage lambda DNA markers (concatemers of 48.5 kb) are visible in panel A (top) and panel B (bottom). **(A)** Distribution of DSBs across the 0.50 Mb *Not*I fragment J near the left end of chromosome 1 (top), and double-cut fragments generated from two meiotic DSBs, visualized by probing between *mbs1* and *mbs2* (bottom). **(B)** Distribution of DSBs across the 1.0 Mb *Not*I fragment E near the middle of chromosome 1 (top), and fragments generated from dual DSBs, visualized by probing between *ura2* and *leu2* (bottom, arrow a-b). **(C)** Distribution of DSBs across the 1.5 Mb *Not*I fragment C near the right end of chromosome 2, and fragments generated from dual DSBs, visualized by a probe at the position indicated (*). **(D)** Distribution of DSBs across the 0.90 Mb *Not*I fragment F near the middle of chromosome 1 (left); MidL (middle) and MidR (right) are separate middle-fragment probes between different pairs of DSB hotspots. The position of all respective double-cut probes are indicated by " ***** " on the DSB lane traces. Note that single-cut fragments are nearly equally frequent in *tel1Δ* and *tel1*$^{+}$ at some hotspots but are more frequent in *tel1Δ* at other hotspots (Table S1). Nevertheless, double-cut fragments are more prominent in *tel1Δ* than in *tel1*$^{+}$ for distances less than about 200 kb (black arrows); longer double-cut fragments are less dependent on Tel1 (white arrows). Quantification of labeled double-cut fragments is in Table S1. Double-cut fragments not labeled were not quantified because of multiple double-cut fragments of similar size, or uncertainty of DSB frequencies.

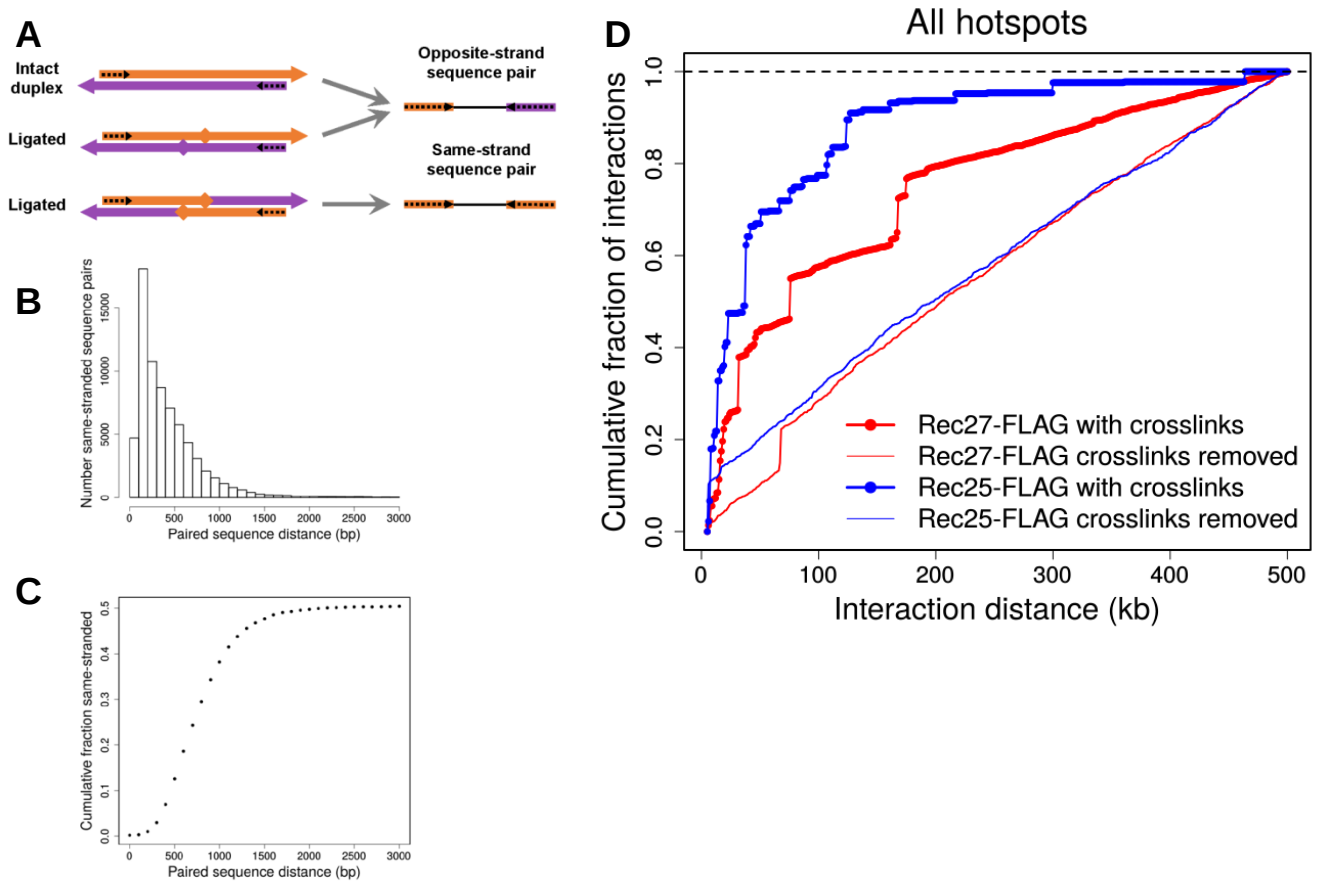

Figure S6. **Analysis of DNA in DSB hotspot clusters.** *Left*: DNA was sheared by sonication to <2 kb and analyzed by high-throughput 3C with IP. **(A)** Ligation of the two ends of one DNA molecule (intra-molecular ligation) gives rise to sequence pairs, from paired-end sequencing, on opposite strands, as do intact, non-ligated DNA molecules. Half of the inter-molecular ligations also give rise to sequence reads on opposite strands, and the other half to reads on the same strand. **(B)** Same-strand reads are highly enriched for short (<2 kb; mode, 100 – 200 bp) distances between reads but with a broad distribution. **(C)** Same-strand reads approach 50% of all reads as the distance between sequence pairs approaches 2 kb, the cutoff used here to ensure sequences were derived from inter-molecular ligations and thus interaction between DSB hotspots. *Right:* Physical clustering of DSB hotspots is limited to an ~200 kb chromosomal region. **(D)** DSB hotspot clustering was analyzed as in Figure 4F but with Rec27-FLAG (red lines) or Rec25-FLAG (blue lines) in place of Rec27-GFP, analyzed in Figures 4 and S1. Data are the summation of ligations between all genomic hotspots with chromatin crosslinks maintained before ligation (lines with data points) or with crosslinks removed just before ligation (lines without data points).

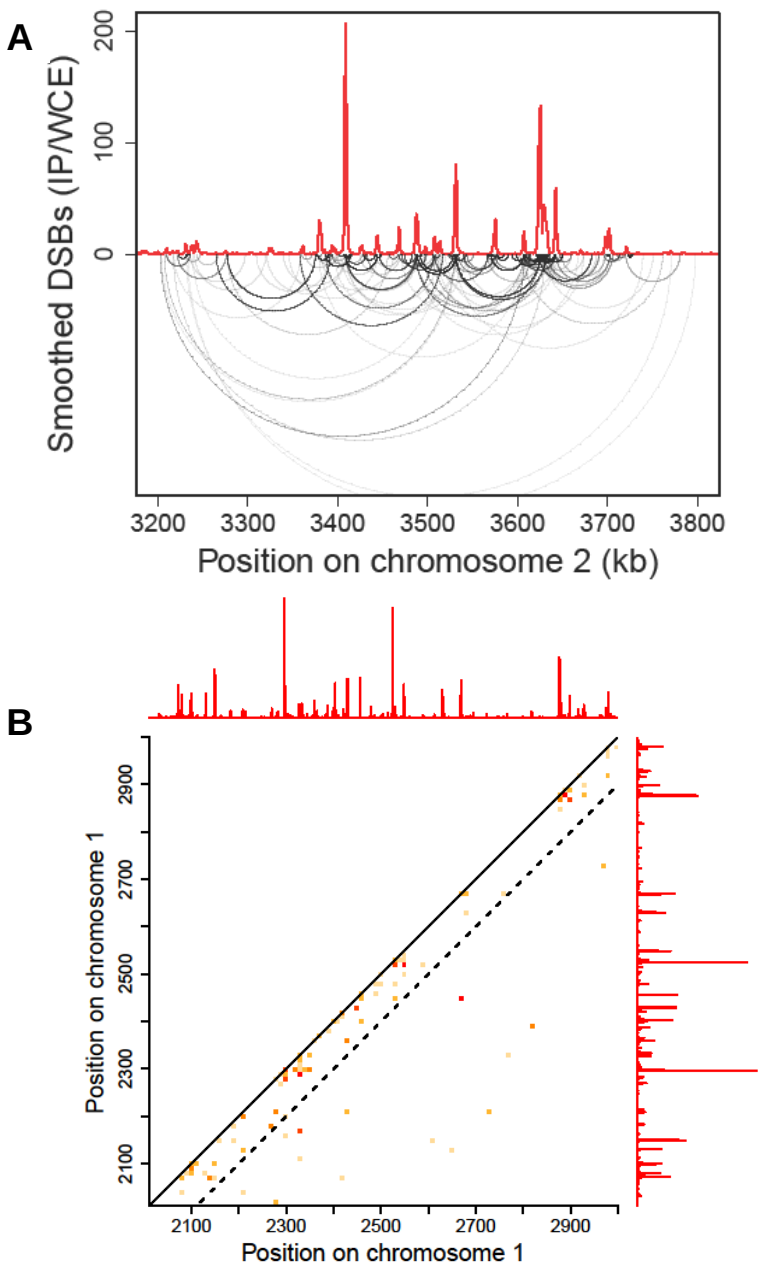

Figure S7. **(A) Analysis of DNA bound by Rec27-GFP**, which binds DSB hotspots with high specificity (1), shows preferential ligation of one hotspot DNA to another hotspot <~100 kb away (lower arcs; frequency indicated by darkness). **(B)** Standard contact heat-map of ligations (hot-hot and hot-cold) across part of chromosome 1. Frequency of ligations (number per kb) is scaled as in Figure 4C. DSB frequency relative to genome median (red line, on a linear scale) is from (6). Note that the map is sparsely populated due to the immunoprecipitation of chromatin and preferential ligations between specific loci (DSB hotspots), and that the greatest density of high-frequency ligations is within about 100 kb (dashed line).

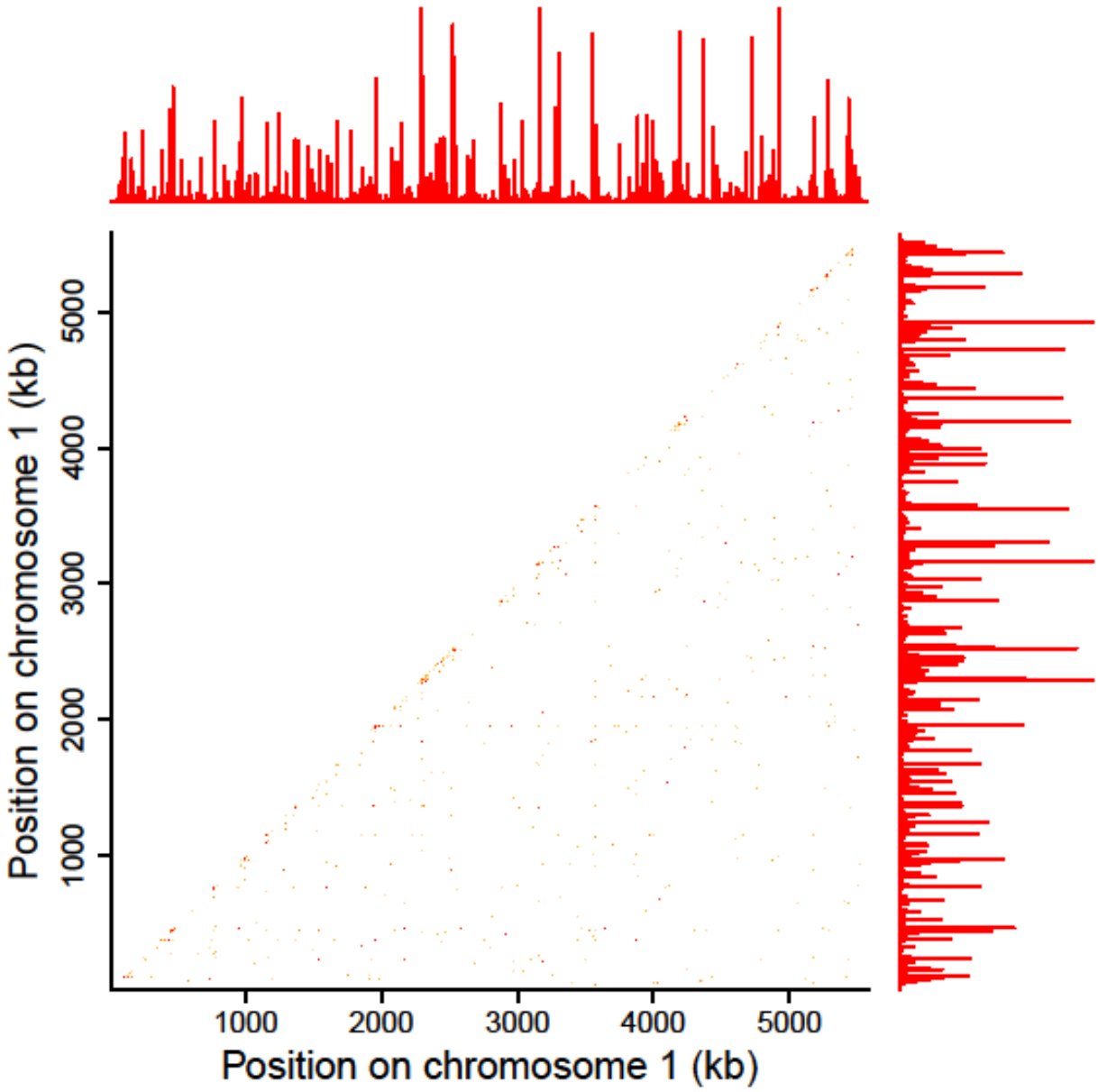

Figure S8. **Standard contact heat-map of ligations (hot-hot and hot-cold) across chromosome 1.** Frequency of ligations (number per kb) is scaled as in Figure 4C. DSB frequency relative to genome median (red line, on a linear scale) is from (6). Note that the map is sparsely populated due to the immunoprecipitation of chromatin and preferential ligations between specific loci (DSB hotspots), and that the greatest density of high-frequency ligations is within about 100 kb.

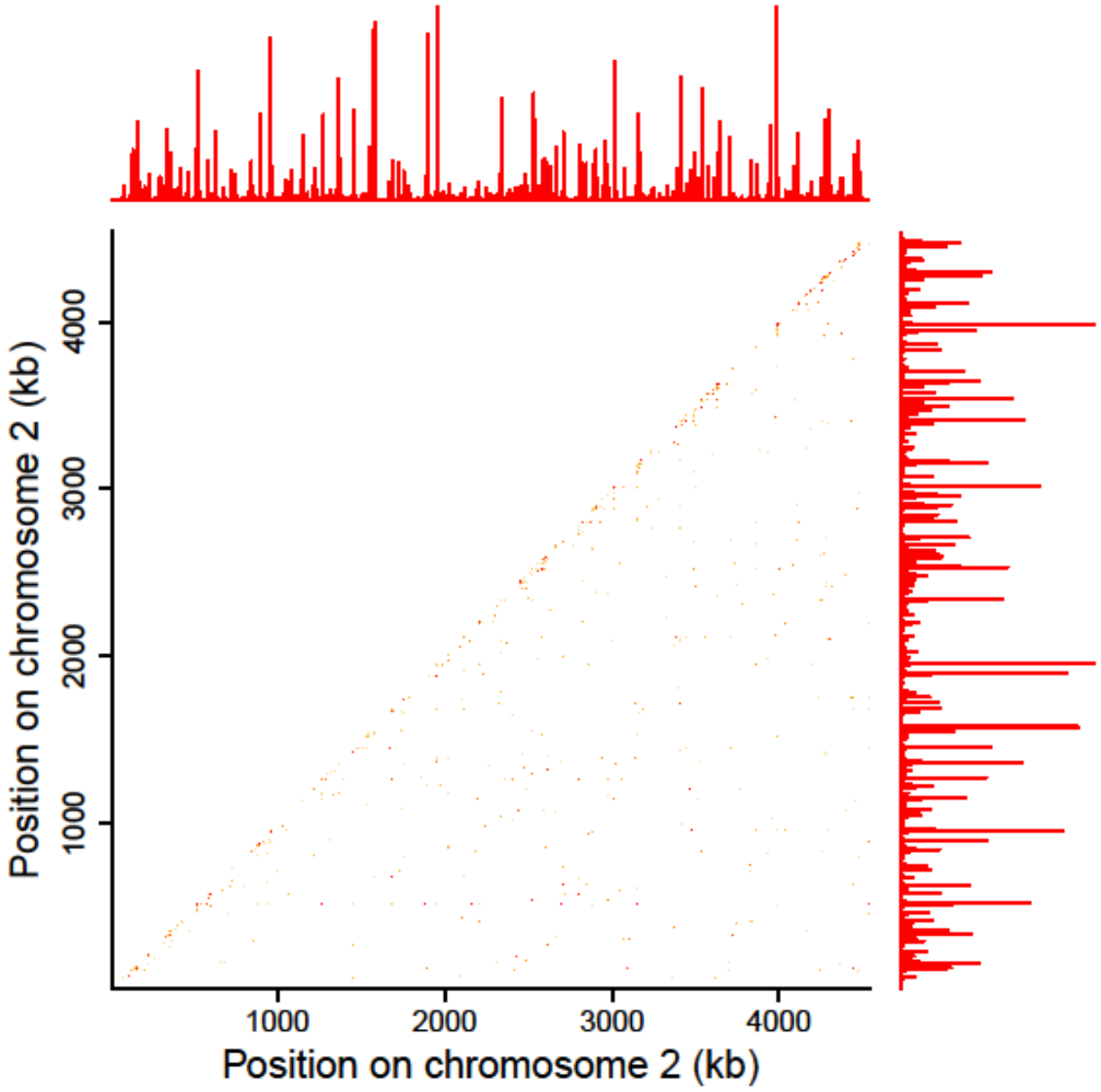

Figure S9. **Standard contact heat-map of ligations (hot-hot and hot-cold) across chromosome 2.** Frequency of ligations (number per kb) is scaled as in Figure 4C. DSB frequency relative to genome median (red line, on a linear scale) is from (6). Note that the map is sparsely populated due to the immunoprecipitation of chromatin and preferential ligations between specific loci (DSB hotspots), and that the greatest density of high-frequency ligations is within about 100 kb.

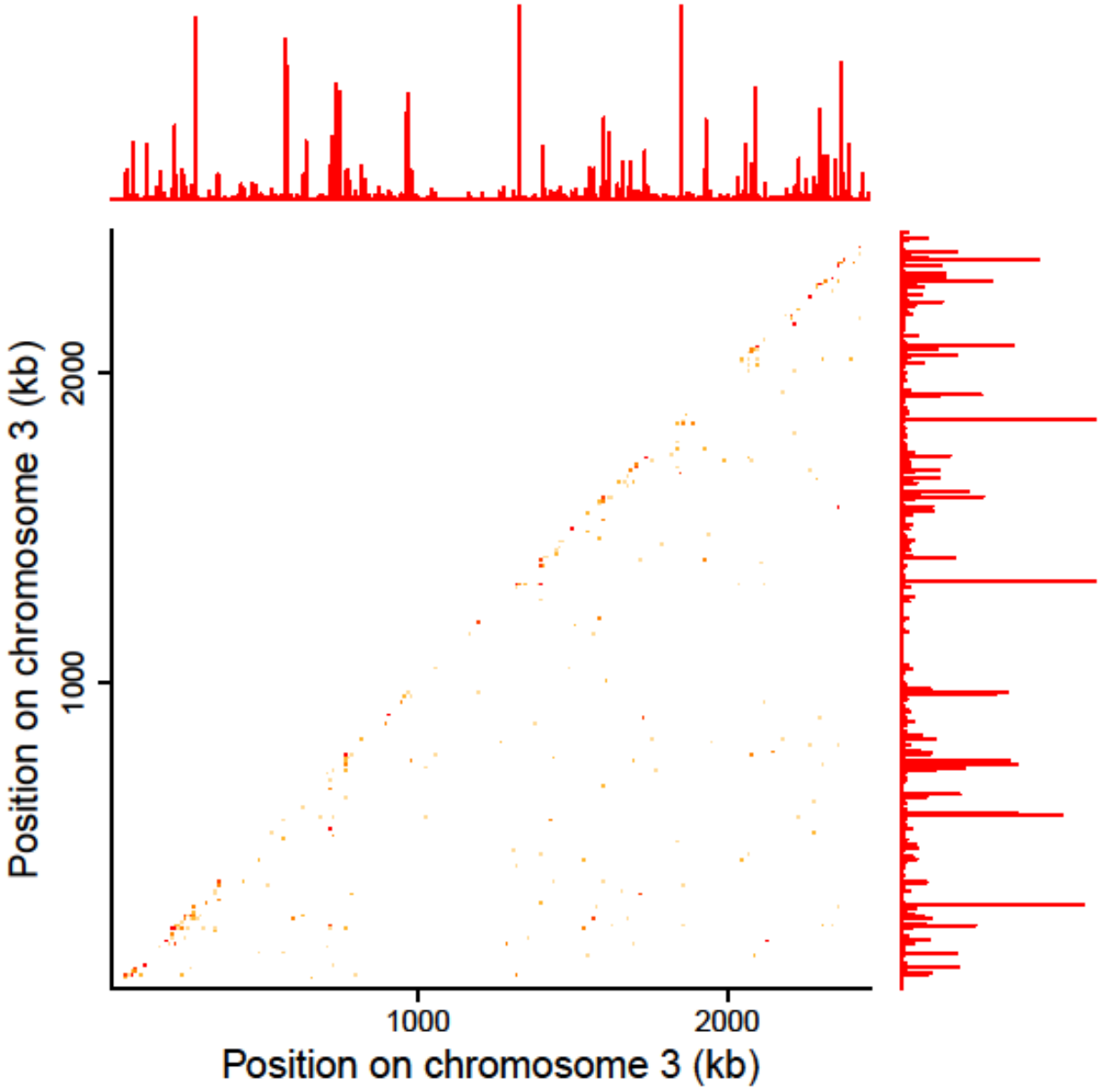

Figure S10. Standard contact heat-map of ligations (hot-hot and hot-cold) across chromosome 3. Frequency of ligations (number per kb) is scaled as in Figure 4C. DSB frequency relative to genome median (red line, on a linear scale) is from (6). Note that the map is sparsely populated due to the immunoprecipitation of chromatin and preferential ligations between specific loci (DSB hotspots), and that the greatest density of high-frequency ligations is within about 100 kb.

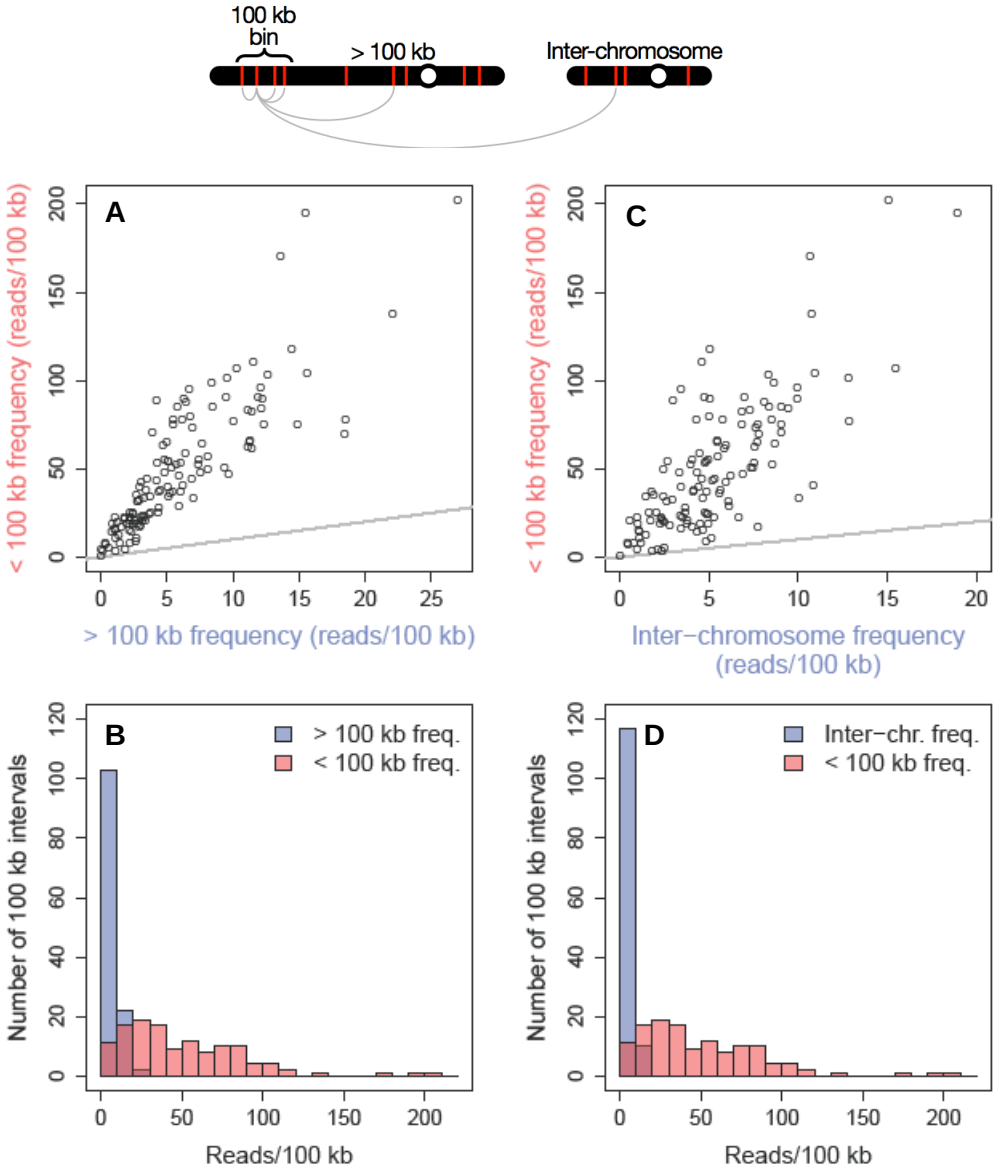

Figure S11. Non-specific ligations between hotspot DNA cannot account for the preferential interactions between hotspots less than 100 kb apart. (A) The genome was divided into 100 kb non-overlapping regions. For each region, sequence read-pairs were compiled if at least one end was in a hotspot within the region and the other in a hotspot on the same chromosome (left part of diagram at top of figure). For each region the number of read-pairs between this region and hotspots >100 kb away was divided by the amount of DNA in hotspots outside this region; similarly, the number of read-pairs between this region and hotspots <100 kb away was divided by the amount of hotspot DNA within this region. These normalized counts were then plotted against one another, with each point representing a 100 kb genomic region. The straight line indicates equality. **(B)** A histogram of the normalized values in panel A. **(C)** As in panel A, but instead compiling sequence read-pairs

between hotspots in each 100 kb region and hotspots on any another chromosome (right part of diagram at top of figure). For each region, the number of read-pairs was divided by the amount of DNA in hotspots on the other chromosomes. This was plotted against the frequency of read-pairs between hotspots <100 kb, as in panel A. **(D)** A histogram of the normalized values used in panel C.

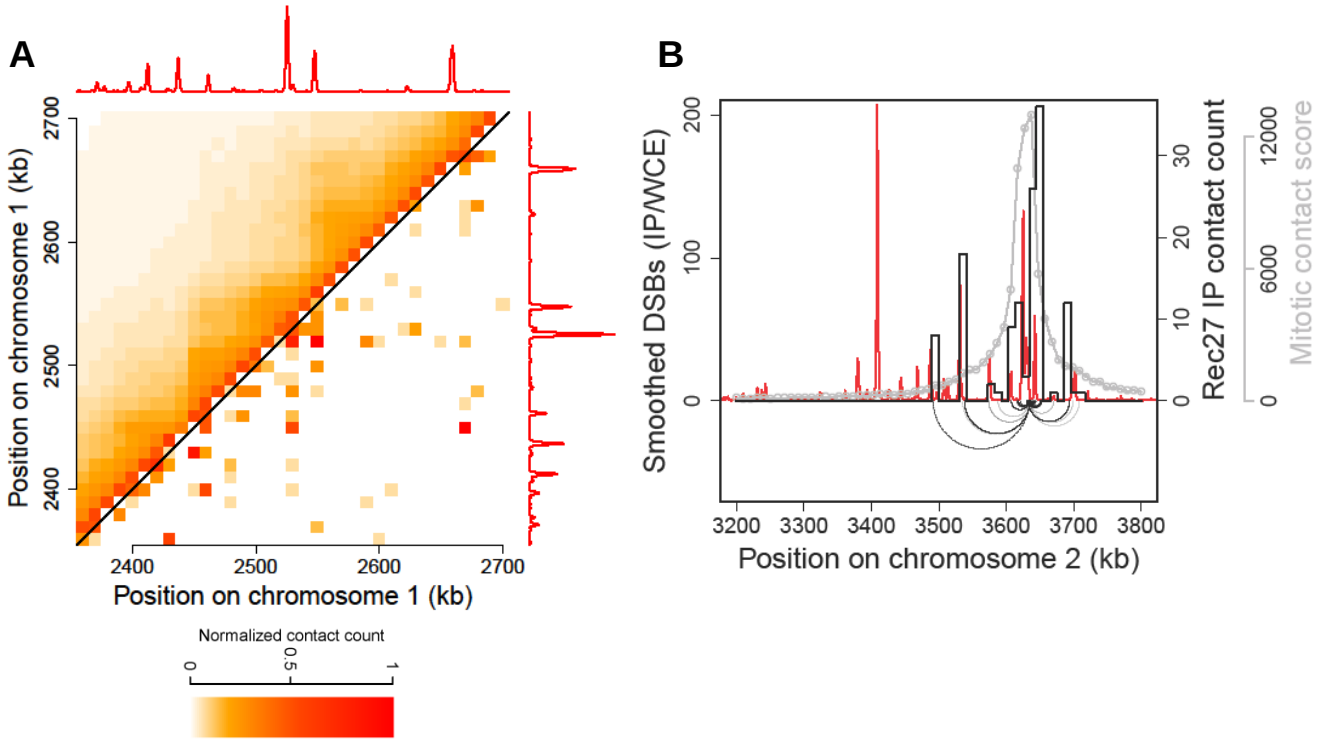

Figure S12. DSB hotspot-hotspot ligations are discontinuous, unlike continuous Hi-C ligations. (A) In this representative genomic interval, Hi-C signals (top left part of panel; ref. 29) indicate domains in which each chromosomal point contacts any other point with a frequency that decreases monotonically with distance, shown by the progressively decreasing darkness of the points indicating 10 kb bins. In sharp contrast, LinE cluster signals (bottom right part of panel) are discontinuous, reflecting preferential ligations between DSB hotspots (indicated by DSB frequency in the graphs above and to the right of the panel) (1). **(B)** The frequency of contacts decreases monotonically with distance in the Hi-C analysis (grey curve) but has multiple peaks in the LinE cluster analysis (bar graph summation of ligations shown by the arcs under DSB hotspots; Figure 4), indicating that DSB hotspots cluster preferentially within chromosomal domains. The similarity of the sizes of domains from the Hi-C data and the sizes of clusters may reflect formation of domains and clusters being influenced by related factors.

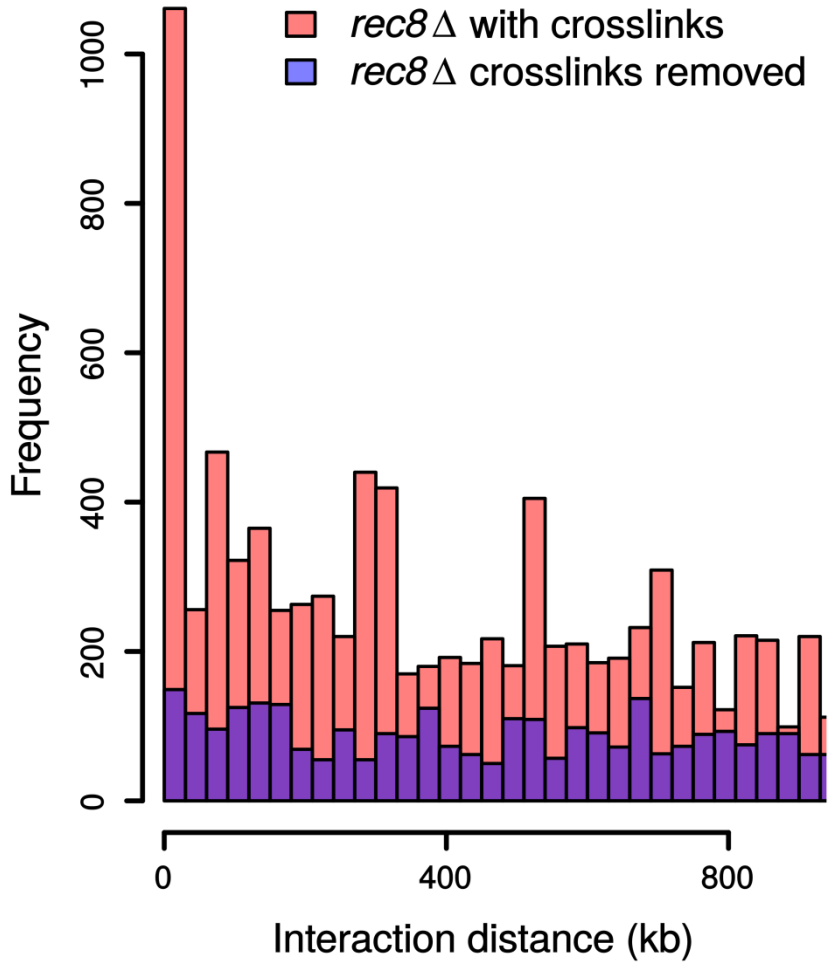

Figure S13. Hotspot interactions are farther apart in the absence of cohesin subunit Rec8. Strain GP8663 (*rec8::kanMX*) was analyzed as in Figure 4E; cumulative curves are in Figure 4F. Data are the frequency of ligations between pairs of sites located the indicated distance apart (in 30 kb bins) among all genomic hotspots with chromatin crosslinks maintained until after ligation (red bars) or with crosslinks removed just before ligation (purple bars).

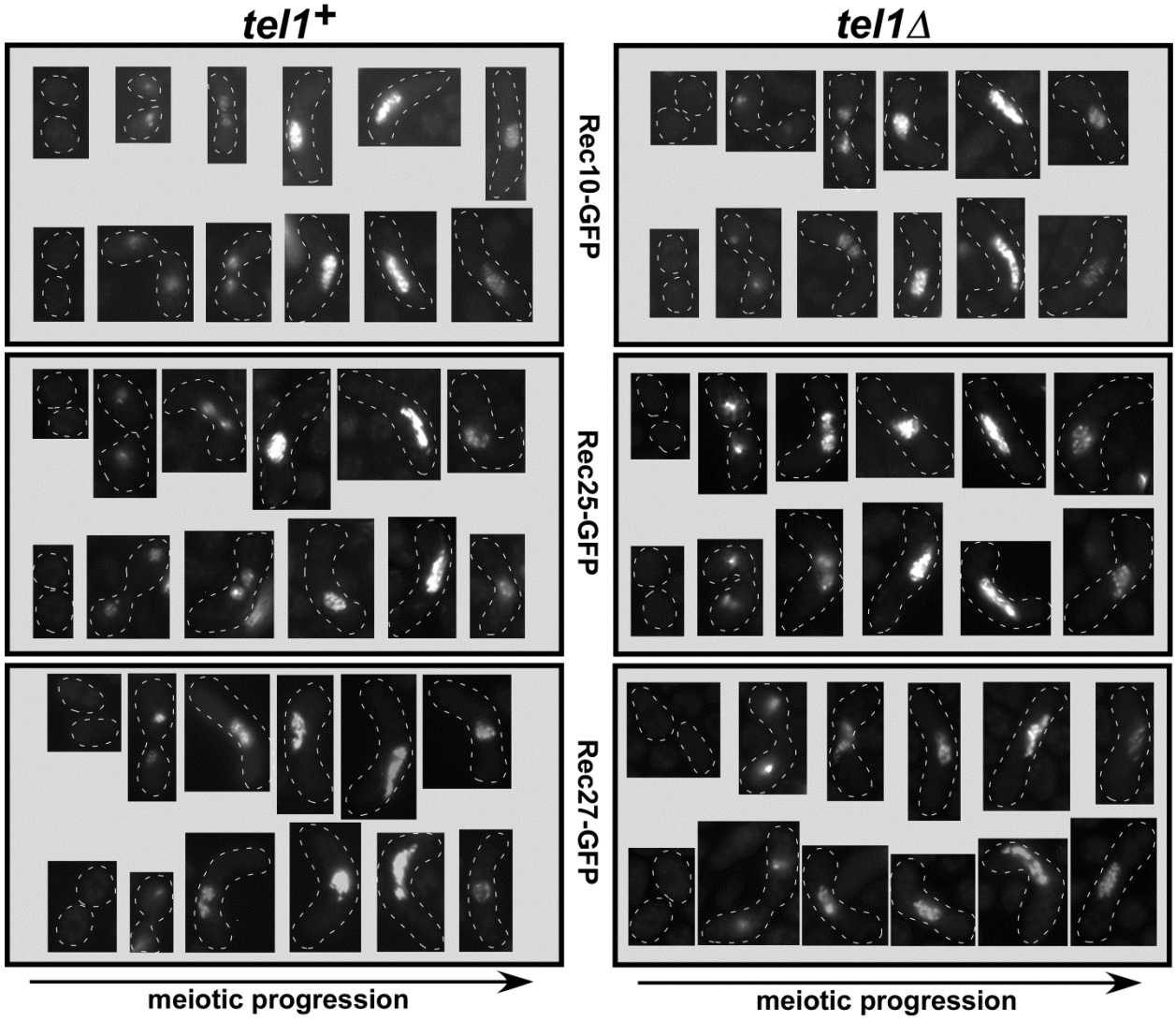

Figure S14. Tel1 DNA damage-response protein kinase is not required for formation of clustered foci of linear element (LinE) proteins Rec10, Rec25, and Rec27. Homothallic (h^{90}) strains with the indicated GFP fusion were spotted on MEA, incubated ~16 hr, and examined by fluorescence microscopy. Images from different cells at various stages of meiosis, in one microscopic field, were arranged in apparent temporal order (left to right). Two such reconstructions are shown for each strain. The stages represented are mating, karyogamy, horsetail movement, and initiation of MI, which occurred at similar frequencies in all strains. Dotted lines indicate the outline of each cell.